

# Preparation and Evaluation of Liquid-Crystal Formulations with Skin-permeation-enhancing Abilities for Entrapped Drugs

Keisuke Yamada<sup>1</sup>, Jun Yamashita<sup>1</sup>, Hiroaki Todo<sup>1</sup>, Keiko Miyamoto<sup>2</sup>, Satoru Hashimoto<sup>2</sup>, Yoshihiro Tokudome<sup>1</sup>, Fumie Hashimoto<sup>1</sup> and Kenji Sugibayashi<sup>1\*</sup>

<sup>1</sup> Faculty of Pharmaceutical Sciences, Josai University (1-1 Keyakidai, Sakado, Saitama 350-0295, JAPAN)

<sup>2</sup> Cosmos Technical Center Co., Ltd. (3-24-3Hasune, Itabashi-ku, Tokyo 174-0046, JAPAN)

**Abstract:** The usefulness of liquid crystals (LC) in topical formulations for application to skin was evaluated by measuring the *in vitro* permeation profile of a model compound, calcein, entrapped in a LC formulation, through excised hairless rat skin and a three-dimensional cultured human-skin model; the viability was determined using the MTT assay. Two physically stable LCs were prepared from a mixture of mono-, di-, and tri-esters 1, and monoesters 2, composed of erythritol and phytanylacetic acid. Cryo-transmission electron microscopy (cryo-TEM), electron diffraction patterns, and small-angle X-ray diffraction (SAXS) observations of the LC nanodispersions showed that the structures of the LCs were reverse hexagonal (LC-A) and cubic (LC-B). The skin-permeation properties of calcein were enhanced by entrapping in the LCs as a result of the increase in calcein partition from the LC dispersion solution into the skin; the properties were analyzed using a skin-permeation–time profile. Drug partitioning could also be modified by the LC structure. No skin damage was caused by the LC formulation in these experiments. The present study suggests that LC dispersions are potential additives in topical drug formulations and cosmetic formulations.

**Key words:** liquid crystal, topical formulation, skin permeation, penetration enhancement

## 1 INTRODUCTION

The primary dosage forms currently used in drug therapy are oral formulations and injections; however, oral formulations have drawbacks such as side effects in the GI tract and the first-pass effect, and injections are painful and may cause infection; transdermal drug delivery systems (TDDS) can avoid these drawbacks. Interestingly, more TDDSs than oral DDSs were developed at the beginning of this century. The outermost layer of the skin, the stratum corneum, acts as a primary barrier against water evaporation from the body and skin permeation of most drugs into the body. Thus, overcoming the stratum corneum barrier is important in advancing the development of TDDSs.

Chemical approaches, such as penetration enhancers<sup>1</sup>, and physical approaches, such as iontophoresis<sup>2</sup>, phonophoresis<sup>3</sup> and electroporation<sup>4,5</sup>, have been evaluated as methods of increasing the skin permeation of several

drugs. Formulation approaches have also been investigated. Liposomes and niosomes are examples of new topical formulations with high penetration activity of entrapped drugs<sup>6-8</sup>; in general, however, such nano-sized materials have poor stability. Recently, solid lipid nanoparticles<sup>9,10</sup> and liquid-crystal (LC) dispersions have been developed for topical formulations; the latter are highly bioadhesive<sup>11</sup> and physically stable. The LC structure is very similar to the intracellular lipid structure in the stratum corneum<sup>12</sup>. Very stable LCs produced from monoolein/oleic acid<sup>13,14</sup> and phytol<sup>15</sup> have been applied to skin and mucosa. LC nanodispersions containing monoolein/oleic acid were used to regulate the skin permeation of indomethacin<sup>16</sup>, cyclosporine<sup>17,18</sup>, vitamin K<sup>19</sup>, and propranolol<sup>20</sup>. These LCs have also been investigated for use in skin-care products<sup>21,22</sup>, and Yamaguchi *et al.* have produced a cubic lipid structure for cosmetic formulations<sup>23</sup>.

In the present study, aqueous dispersions of LCs con-

\*Correspondence to: Kenji Sugibayashi, Faculty of Pharmaceutical Sciences, Josai University, 1-1 Keyakidai, Sakado, Saitama 350-0295, JAPAN

E-mail: sugib@josai.ac.jp

Accepted July 28, 2010 (received for review May 16, 2010)

Journal of Oleo Science ISSN 1345-8957 print / ISSN 1347-3352 online  
<http://www.jstage.jst.go.jp/browse/jos/>

taining sodium calcein as a model penetrant were prepared using a mixture of mono-, di-, and tri-esters **1** and monoesters **2**, composed of erythritol and phytanylacetic acid. The permeation profiles of this model compound were measured using excised hairless rat skin and a three-dimensional cultured human-skin model<sup>24</sup>, living skin equivalent-high (LSE-high), to evaluate the effects of the LC structures. Two kinds of LC were used to make aqueous dispersions.

## 2 EXPERIMENTAL PROCEDURES

### 2.1 Materials

Erythritol and sodium calcein (623 Da,  $\log K_{ow} = -3.5$ ) were purchased from Tokyo Chemical Industries Co., Ltd. (Tokyo, Japan). *t*-Butyl methyl ether was purchased from Kanto Chemical Co., Inc. (Tokyo, Japan). Methyl 5,9,13,17-tetramethyloctadecanoate was prepared by the Johnson transfer reaction. EDTA · 2Na was obtained from Dojin Molecular Technologies, Inc. (Mashiki, Kumamoto, Japan). A surfactant, Pluronic F127, was purchased from BASF (Ludwigshafen, Germany). Other reagents and solvents were of special grade or HPLC grade and used without further purification.

### 2.2 Preparation of a mixture of mono-, di-, and tri-esters **1** and monoesters **2**, composed of erythritol and phytanylacetic acid

Erythritol (2.50 kg) was dissolved in dimethyl sulfoxide (10.8 kg) at 100°C under nitrogen purging before addition of anhydrous CaCO<sub>3</sub> (37.8 g) at 80°C. Methyl phytanylacetate (5,9,13,17-tetramethyloctadecanoate) (4.83 kg) was added dropwise to the solution under reduced pressure over 2.5 h. The reaction mixture was refluxed under reduced pressure overnight, while the methanol produced

was gradually removed by distillation. After cooling, the mixture was neutralized by addition of formic acid (29 g), and concentrated *in vacuo*. The residue (6.1 kg) was diluted with *t*-butyl methyl ether (18.3 kg), and filtered to remove the remaining erythritol. The filtrate was diluted again with *t*-butyl methyl ether (24 kg), washed twice with aqueous NaHCO<sub>3</sub>, and concentrated *in vacuo* at 100°C. The product obtained (4.7 kg, **1**) consisted of monoesters (36%), diesters (12%), and triesters (52%) of erythritol and phytanylacetic acid (the ratio was determined by GC analysis). The mixture **1** was purified by column chromatography using silica gel (Wakogel C-300; Wako Pure Chemicals Co., Ltd., Osaka, Japan) to afford monoesters **2** of 1-*O*- and 2-*O*-phytanylacetylerythritol.

### 2.3 Experimental animals and three-dimensional cultured human-skin models

Male hairless rats (WBM/ILA-Ht, 200-250 g b.w.) were obtained from the Life Science Research Center, Josai University (Sakado, Saitama, Japan) or Ishikawa Experimental Laboratories (Fukaya, Saitama, Japan). Animal breeding and experiments were conducted according to the Josai University guidelines.

A three-dimensional cultured human-skin model, Living Skin Equivalent-high (LSE-high)<sup>24</sup>, was obtained from Toyobo (Osaka, Japan).

### 2.4 Preparation of liquid-crystal dispersions

Table 1 shows the prescriptions for liquid crystal A (LC-A) and liquid crystal B (LC-B) nanodispersions. Ten grams of crude ester **1** or pure ester **2** were used to prepare LC-A and LC-B, respectively. In this step, LC-A and LC-B were semisolid and were nanodispersed, using a high pressure emulsifier (NM2-L200AR; Yoshida Kikai Co., Ltd, Nagoya, Japan) or an ultrasonic homogenizer (USP-50; Shimadzu Corp., Kyoto, Japan), in an aqueous solution (90.0

**Table 1** Prescription to make liquid crystal dispersion

Ingredients	30 mM	Blank	30 mM	Blank
	calcein-entrapped LC-A (%)	LC-A (%)	calcein-entrapped LC-B (%)	LC-B (%)
1- <i>o</i> -(5,9,13,17-tetramethyloctadecanoyl)erythritol (crude, <b>1</b> )	10.0	10.0	–	–
1- <i>o</i> -(5,9,13,17-tetramethyloctadecanoyl)erythritol (pure, <b>2</b> )	–	–	10.0	10.0
sodium calcein	2.0	–	2.0	–
Pluronic F127 (10%)	10.0	10.0	10.0	10.0
methyl <i>p</i> -hydroxyl benzoate	0.1	0.1	0.1	0.1
purified water	77.9	79.9	77.9	79.9
Total	100	100	100	100

g) containing sodium calcein, Pluronic F127, and methyl *p*-hydroxybenzoate. The calcein concentrations in LC-A and LC-B were different (see Table 1).

## 2.5 Measurement of physical properties of liquid crystals

### 2.5.1 X-ray analysis

X-ray diffraction analyses were performed on a small-angle X-ray diffraction system (SAXSess) equipped with a temperature controller (TCS 120), a PW3830 X-ray generator (Cu-K $\alpha$ , 0.1542 nm wavelength) (AntonPaar Japan Co., Ltd., Tokyo, Japan), and an image plate detector (Perkin Elmer Japan Co., Ltd., Yokohama, Japan). Diffraction analyses were performed using a vacuum-resistant glass capillary cell at 25°C for 2 h. The obtained SAXS patterns were plotted against the scattering vector length,  $q = (4\pi/\lambda) \sin(\theta/2)$ , where  $\theta$  is the scattering angle. The scattering intensity was normalized by the decayed direct beam intensity.

### 2.5.2 Observations by cryo-TEM

The prepared LC dispersions were observed by cryo-transmission electron microscopy (cryo-TEM) (JEM-2011, JEOL Ltd., Akishima, Tokyo, Japan). LC dispersion samples for cryo-TEM observations were rapidly frozen on a microgrid with 1-5  $\mu\text{m}$  pores at approximately  $-175^\circ\text{C}$ , with ethane as the freezing solvent, using a rapid freezing system (Leica Microsystems Japan, Tokyo, Japan). The observations were performed at Terrabase Co., Ltd. (Okazaki, Aichi, Japan).

### 2.5.3 Determination of calcein entrapping ratios

The calcein entrapping ratios in LC-A and LC-B were determined using a centrifuge (CS100GXII; Hitachi Koki Co., Ltd., Tokyo, Japan). LC-A or LC-B (1.0 mL) in a tube was placed in an angle rotor (S120 AT2; Hitachi Koki Co., Ltd.). After centrifugation, the external phase (aqueous phase), which separated from the LC phase, was withdrawn and the amount of calcein was determined, after adequately diluting with pH 7.4 phosphate buffer containing 1 mM EDTA  $\cdot$  2Na, at 488 nm and 515 nm excitation and emission wavelengths, respectively, by a fluorescence spectrophotometer (RF-5300PC; Shimadzu Corp., Kyoto, Japan).

The entrapping ratio was determined by the following equation:

$$\text{Entrapped ratio (\% w/w)} = \frac{\text{total drug amount} - \text{drug amount in external phase}}{\text{total drug amount}} \times 100 \quad (1)$$

### 2.5.4 Measurement of droplet diameter of liquid-crystal dispersions

The prepared LC dispersions were diluted with distilled water; 1.0 mL was transferred to a disposable plastic cell set in a Zeta Sizer 3000HSA (Otsuka Electronics Co., Ltd., Hirakata, Osaka, Japan) to determine the droplet diameter by dynamic light scattering.

## 2.6 In vitro skin-permeation experiments

We selected three types of membrane-intact and stripped hairless rat skins, and LSE-high to evaluate the enhancement effect of the LC formulations. These membranes represented healthy intact skin, damaged skin, and appendage-free skin. The left and right sides of the abdominal skin were excised from hairless rats under anesthesia using *i.p.* injections of sodium pentobarbital (50 mg/kg). Stripped skin was prepared by tape-stripping the stratum corneum 20 times using adhesive cellophane tape (Nichiban Co., Ltd., Tokyo, Japan). After excising the skin, superfluous subcutaneous fat was carefully trimmed off. The three-dimensional cultured human-skin model, LSE-high, was washed with physiological saline and separated from the well.

Each obtained skin membrane was set in a Franz-type diffusion cell with an effective diffusion area of 1.77 cm<sup>2</sup> or 0.78 cm<sup>2</sup> for hairless rat skin or LSE-high, respectively. To decrease the endogenous fluorescence of the skin and the dryness of the stratum corneum, 1.0 mL of physiological saline and 6 mL of pH 7.4 phosphate buffer containing 1.0 mM EDTA  $\cdot$  2Na were added to the stratum corneum and dermis side, respectively, and the skin sample was maintained for 1.0 h. Calcein (1.0 mL) and fresh buffer (6.0 mL) were then placed on each side of the skin to start the permeation experiments. The system was maintained at 32°C, and the receiver compartment was agitated by a magnetic stirrer. The receiver sample (0.5 mL) was periodically sampled to measure the skin permeation of calcein, and an equivalent volume of saline was added to keep the volume constant.

## 2.7 Determination of calcein concentration

The receiver sample was centrifuged and diluted with pH 7.4 phosphate buffer containing 1.0 mM EDTA  $\cdot$  2Na. The calcein concentration in the sample was determined by fluorescence spectrophotometry, as described in section 2.5.3.

## 2.8 Determination of permeation parameters

The rate-limiting steps of calcein permeation through hairless rat skin and LSE-high are permeation through the stratum corneum and permeation through the whole epidermis, respectively<sup>24</sup>. Both membrane permeation profiles, however, can be analyzed as a one-layered diffusion membrane. In the present experiments, the receiver solution was always assumed to be in the sink condition. Equations (2)-(4) can be written using Fick's law of diffusion;  $P$ , the permeability coefficient,  $D$ , the diffusion coefficient in the skin barrier, and  $K$ , the partition coefficient from the donor compartment to the skin barrier, were determined<sup>25</sup>. The thicknesses of the intact and stripped hairless rat skin, and of LSE-high were 20  $\mu\text{m}$ , 580  $\mu\text{m}$ , and 20  $\mu\text{m}$ , respectively<sup>24, 26</sup>.

$$t_{lag} = \frac{L^2}{6D} \quad (2)$$

$$J_{ss} = \frac{DKC_d}{L} \quad (3)$$

$$P = \frac{DK}{L} \quad (4)$$

In the equations,  $t_{lag}$  is the lag time to reach steady-state skin-permeation,  $J_{ss}$  is the steady-state flux, and  $C_d$  is the concentration of calcein in the donor solution.

## 2.9 Preparation of skin slices

After the permeation experiments, the intact and stripped hairless rat skin and the LSE-high were washed with pH 7.4 phosphate buffer containing EDTA · 2Na at a concentration of 1 mM. Each sample was then embedded in Tissue-Tek® OTC compound (Sakura Fine Tech Japan Co., Ltd., Tokyo, Japan) and frozen in isopentane using liquid nitrogen at  $-20^\circ\text{C}$ . The frozen tissues were sliced into horizontal slices of about 20  $\mu\text{m}$  using a Cryostat (CM3050S; Leica Microsystems Japan). The specimens were observed under a fluorescence microscope.

## 2.10 MTT assay

Skin irritation caused by the LC dispersions was evaluated by skin viability using the MTT [3-(4,5-dimethylthiazol-2-yl)-2,5-diphenyltetrazolium bromide] assay<sup>27,28</sup>. Calcein-free LC-A and LC-B dispersions, and 2% Pluronic F127 solution were evaluated. Distilled water and 10% sodium dodecyl sulfate (SDS) were used as negative and positive controls, respectively. The samples (0.5 mL each) were applied in a glass chamber with an effective diffusion area of 1.0  $\text{cm}^2$  to the abdominal skin (intact or stripped) of hairless rats, anesthetized by *i.p.* injections of urethane at a dose of 1.0 g/kg, for 8 h. The treated skin sites were excised and a 6.0-mm diameter skin sample was obtained using a biopsy punch. MTT solution (2.0 mL) was added to an assay tray containing the skin sample and incubated at  $37^\circ\text{C}$  under bubbled  $\text{CO}_2/\text{O}_2$  (5%/95%). The MTT was adjusted to 0.333 mg/mL using DMEM medium. After incubation, excess MTT was washed off with distilled water and the skin sample was moved to a microtube. 0.04 N HCl-isopropyl alcohol (1.0 mL) was added to the tube; the skin was minced using scissors. The samples were kept for 12 h with agitation to extract formazan. The obtained formazan was spectrophotometrically determined at 570 nm. The obtained value was adjusted with respect to skin weight.

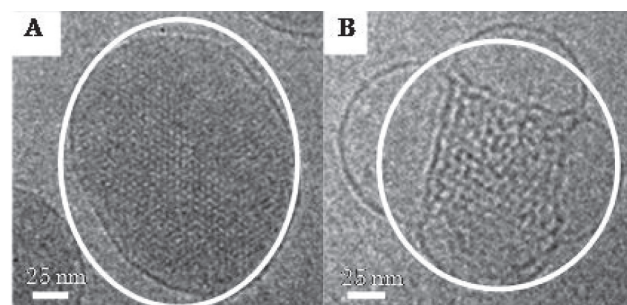
## 2.11 Statistical analysis

The Mann-Whitney U-test was used for statistical analysis of the cumulative amount of calcein permeating the skin, and viability of the cutaneous cells.  $P < 0.05$  was considered to be significant.

## 3 RESULTS AND DISCUSSION

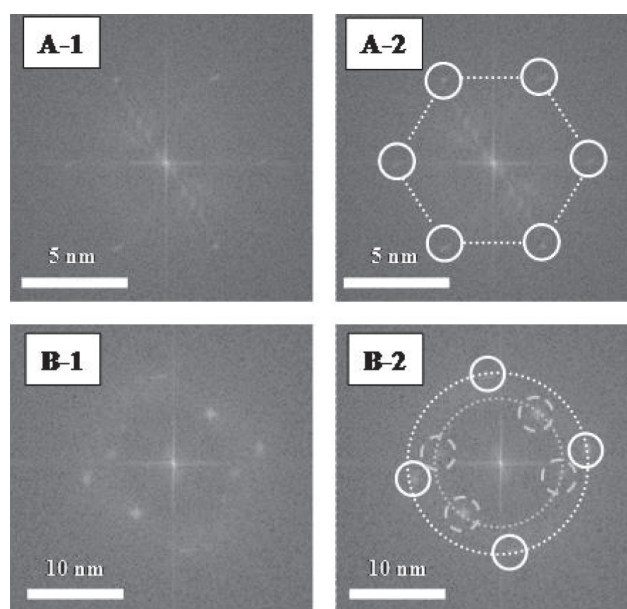
### 3.1 Analysis of structure of liquid-crystal dispersions

Figure 1 shows cryo-TEM photographs of LC-A and



**Fig. 1** Cryo-TEM microscope images of liquid-crystal phase dispersions.

Photographs A and B are LC-A and LC-B, respectively. LC structures were found in the circles of both A and B. Each white bar indicates a length of 25 nm.



**Fig. 2** Electron diffraction patterns of liquid-crystal phase dispersions.

A-1 and A-2, and B-1 and B-2 show the same photographs of LC-A and LC-B, respectively, without and with auxiliary lines and marks. A-2 shows hexagonal LC with a 4.6 nm periodic structure. LC-B shows cubic LC with two periodic structures of cycles 6.0 nm and 9.0 nm. Each white bar indicates a length of 5 nm or 10 nm.

LC-B. As in the case of cryo-TEM photographs of cubic LCs prepared from monoolein and oleic acids<sup>13,14</sup>, LC structures were observed in Pluronic solutions of LC-A and LC-B in the present study (white circles in Fig. 1). Figure 2 shows the electronic diffraction patterns of the LCs determined from the cryo-TEM photographs. It was found from these diffraction patterns that LC-A was hexagonal, with a 4.6 nm periodic structure (A-2 dashed lines in Fig. 2), and LC-B was cubic, with two periodic structures of cycles 6.0 nm and 9.0 nm (B-2 dashed lines in Fig. 2).

SAXS patterns were used to determine the LC structures. The crystal structures and lattice parameters can be determined from the interlayer spacing. Figure 3 shows the observed X-ray diffraction profiles of LC-A and LC-B nanodispersions, and Table 2 summarizes the peak positions and ratios of the diffraction spacings. In general, an LC has a specific diffraction spacing ratio, and each value is shown in Table 2<sup>29</sup>. The diffraction spacing ratio was 1:0.572:0.494... for blank LC-A and 1:0.577:0.497... for calcein-entrapped LC-A. These ratios were very similar to each other and also to 1:  $\sqrt{1/3}$  :  $\sqrt{1/4}$  :  $\sqrt{1/7}$ , the values for hexagonal/reverse-hexagonal LCs, suggesting that the LC formulation prepared from crude terpenoid ester 1 must be reverse hexagonal. The diffraction spacing ratio was 1:0.697:0.572... for blank LC-B, and 1:0.730:0.591... for calcein-entrapped LC-B. These ratios are similar to that of a cubic (bicontinuous) LC structure (1:  $\sqrt{3/4}$  :  $\sqrt{3/8}$  :  $\sqrt{3/11}$ ).

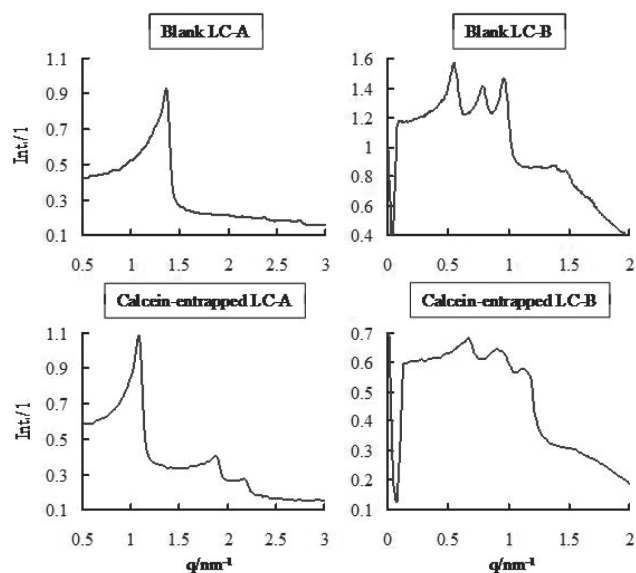


Fig. 3 Small-angle X-ray diffraction pattern of each liquid-crystal dispersion.

### 3.2 Evaluation of physicochemical properties of liquid-crystal dispersions

Table 3 shows the physicochemical properties of the LC nanodispersions prepared in this experiment. No great dif-

Table 2 Peak position ( $q/\text{nm}^{-1}$ ), surface separation ( $d/\text{nm}^{-1}$ ) and ratio of diffraction spacing ( $dk/d_1$ ) observed in Bragg reflection

	Peak position ( $q/\text{nm}^{-1}$ )	interlayer spacing ( $d/\text{nm}^{-1}$ )	Spacing ratio* ( $dk/d_1$ )
Blank LC-A	1.354	4.640	1.0
	2.368	2.653	0.572
	2.743	2.291	0.494
Calcein-entrapped LC-A	1.083	5.800	1.0
	1.878	3.346	0.577
	2.178	2.885	0.497
Blank LC-B	0.550	11.424	1.0
	0.789	7.965	0.697
	0.961	6.537	0.572
Calcein-entrapped LC-B	1.354	4.640	1
	2.368	2.653	0.730
	2.743	2.291	0.591

\* LC structure of spacing ratio ( $dk/d_1$ )

Hexagonal and reverse hexagonal LC: 1:  $\sqrt{1/3}$  :  $\sqrt{1/4}$  :  $\sqrt{1/7}$

Cubic LC (bicontinuous): 1:  $\sqrt{3/4}$  :  $\sqrt{3/8}$  :  $\sqrt{3/11}$

(discontinuous): 1:  $\sqrt{1/2}$  :  $\sqrt{1/3}$  :  $\sqrt{1/4}$

Lamellar: 1:  $1/2$  :  $1/3$  :  $1/4$

**Table 3** Diameter (nm) of liquid crystal and entrapping ratio (%) of calcein in liquid crystal dispersion

	Diameter (nm)	Entrapping ratio (%)
Calcein-entrapped LC-A	250.0	8.26 ± 0.66
Blank LC-A	253.2	–
Calcein-entrapped LC	293.6	14.02 ± 1.54
Blank LC-B	287.0	–

ference was observed between the particle diameters of the LC-A and LC-B formulations. The blank LC formulations were white and turbid for both LC-A and LC-B. The calcein-entrapping ratio in LC-A was much higher than that in LC-B. If we use another compound of different lipophilicity and molecular weight, the entrapping ratio may be different. The present blank LC formulations were very stable for a long time period, as evaluated by their particle diameters and X-ray diffraction pattern.

### 3.3 Skin-penetration-enhancing effect of liquid crystals

Figure 4 shows the time course of calcein permeation through excised hairless rat skin from reverse-hexagonal liquid crystal (LC-A) formulations. In intact and stripped skin, the skin permeations of calcein in the LC-A formulation were 3 times and 10 times higher, respectively, than the permeation of free calcein. In addition, the mixture of LC-A dispersion and free calcein showed similar skin permeation to that of free calcein solution. Thus, the blank LC formulation itself did not have any penetration-enhancement effect. The surfactant Pluronic F-127 did not show any enhancement effect (data not shown). Permeation parameters were determined by the time course of the cumulative level of skin permeation. The calculated parameters are shown in Table 4. The partition coefficient,  $K$ , was markedly increased by addition of the LC-A formulation, suggesting that LC-A is highly distributed from the disper-

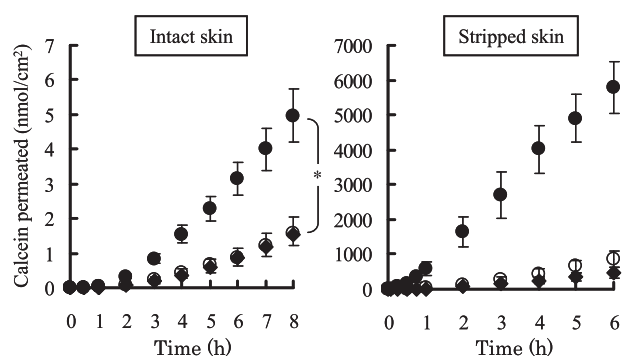


**Fig. 4** Effect of LC-A formulation on the time course of the cumulative amount of calcein that permeated hairless rat intact and stripped skin. Symbols are as follows:  $\blacklozenge$ : free calcein;  $\circ$ : free calcein plus blank LC-A;  $\bullet$ : calcein-entrapped LC-A. Asterisks indicate a significant difference between calcein-entrapped LC-A and free calcein groups ( $p < 0.05$ ). Each point represents the mean  $\pm$  S.E. of at least 3-7 experiments.

sion to the skin surface (stratum corneum).

Next, the time course of skin permeation of calcein from the cubic liquid-crystal dispersion (LC-B) was evaluated; the results are shown in Fig. 5. Enhanced permeation of

**Table 4** Partition coefficient ( $K$ ), diffusion coefficient ( $D$ ), and permeability coefficient ( $P$ ) through hairless rat skin after application of LC-A

	30 mM calcein	calcein-entrapped LC-A	physical mixture
intact skin			
$K$	0.10 ± 0.02	0.22 ± 0.04	0.09 ± 0.03
$D$ ( $\times 10^{-11}$ cm <sup>2</sup> /s)	6.05 ± 0.52	7.54 ± 0.18	6.75 ± 0.68
$P$ ( $\times 10^{-9}$ cm/s)	2.91 ± 0.55	8.32 ± 1.33	2.80 ± 0.91
stripped skin			
$K$	0.52 ± 0.13	2.51 ± 0.87	1.19 ± 0.20
$D$ ( $\times 10^{-7}$ cm <sup>2</sup> /s)	1.04 ± 0.07	3.22 ± 1.14	0.89 ± 0.07
$P$ ( $\times 10^{-7}$ cm/s)	9.41 ± 2.86	110 ± 12.5	18.9 ± 4.51

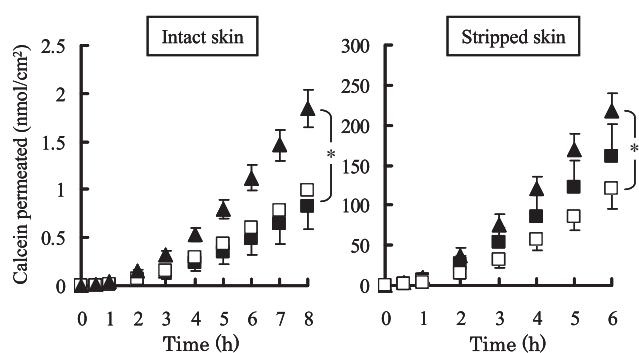


**Fig. 5** Effect of LC-B formulation on the time course of the cumulative amount of calcein that permeated hairless rat intact and stripped skin. Symbols are as follows: ■: free calcein; □: free calcein plus blank LC-B; ▲: calcein-entrapped LC-B. Asterisks indicate a significant difference between calcein-entrapped LC-A and free calcein groups ( $p < 0.05$ ). Each point represents the mean  $\pm$  S.E. of at least 3-12 experiments.

calcein through hairless rat skin was observed with LC-B as well as with LC-A; **Table 5** summarizes the permeation parameters for LC-B. Increased partition of calcein was observed with LC-B, as well as with LC-A. No partition increase was observed for stripped skin with LC-B, unlike the case with LC-A. Determination of the physical and chemical properties of LC-A and LC-B is difficult, and the ratio of LC in each formulation was uncertain. LC-A had a high affinity for both the stratum corneum and the viable epidermis, whereas LC-B showed a high affinity for the stratum corneum, but not for the viable epidermis. Identification of suitable LCs is an issue which needs to be discussed.

Similar permeation experiments were carried out using a three-dimensional cultured human-skin model, LSE-high.

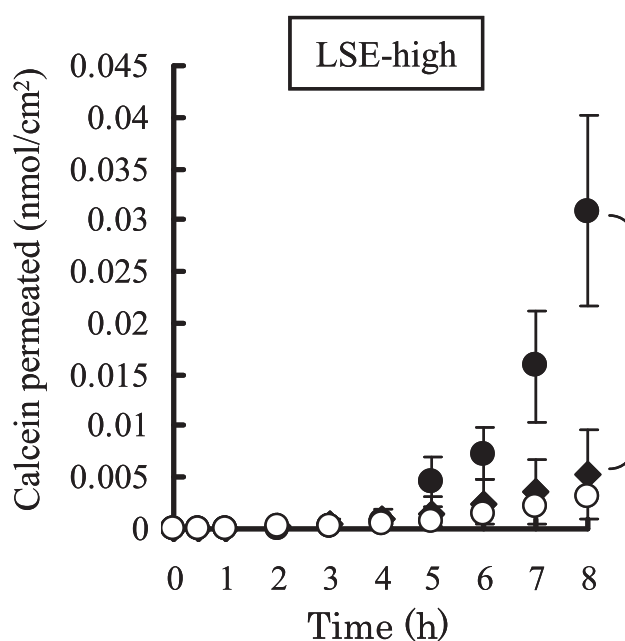


**Fig. 6** Effect of LC-A formulation on the time course of the cumulative amount of calcein that permeated LSE-high. Symbols are as follows: ◆: free calcein; ○: free calcein plus blank LC-A; ●: calcein-entrapped LC-A. Asterisks indicate a significant difference between calcein-entrapped LC-A and free calcein groups ( $p < 0.05$ ). Each point represents the mean  $\pm$  S.E. of at least 3-4 experiments.

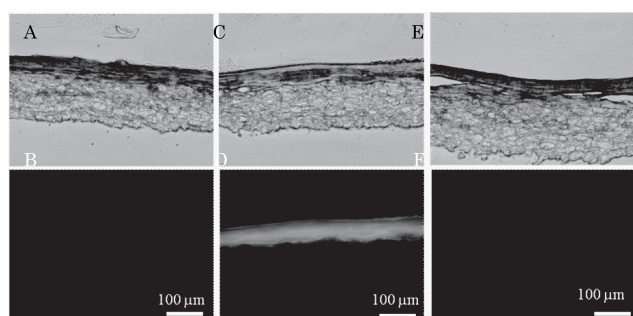
The data are shown in **Fig. 6** and **Table 6**. LC-A showed a high enhancement effect on the skin permeation of calcein. Since LC would increase the partitioning of an entrapped drug into the stratum corneum, the penetration-enhancement effect by LC formulations would also be obtained for the stratum corneum barrier.

**Table 5** Partition coefficient ( $K$ ), diffusion coefficient ( $D$ ), and permeability coefficient ( $P$ ) through hairless rat skin after application of LC-B

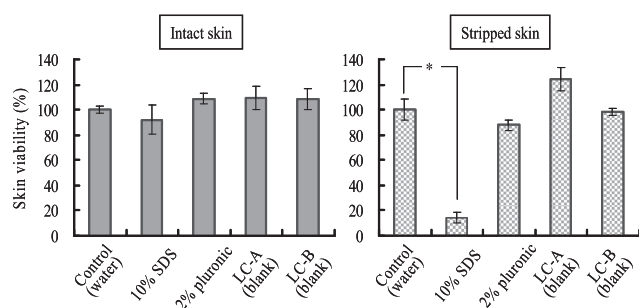
	3 mM calcein	calcein-entrapped LC-B	physical mixture
intact skin			
$K$	0.53 $\pm$ 0.12	0.59 $\pm$ 0.11	0.95 $\pm$ 0.10
$D$ ( $\times 10^{-11}$ cm <sup>2</sup> /s)	5.95 $\pm$ 0.78	6.47 $\pm$ 0.74	6.94 $\pm$ 0.39
$P$ ( $\times 10^{-8}$ cm/s)	1.56 $\pm$ 0.38	1.84 $\pm$ 0.13	3.23 $\pm$ 0.32
stripped skin			
$K$	2.18 $\pm$ 0.08	2.44 $\pm$ 0.39	2.53 $\pm$ 0.26
$D$ ( $\times 10^{-8}$ cm <sup>2</sup> /s)	9.04 $\pm$ 1.33	6.92 $\pm$ 2.83	10.7 $\pm$ 1.45
$P$ ( $\times 10^{-6}$ cm/s)	3.46 $\pm$ 0.65	2.95 $\pm$ 0.55	4.48 $\pm$ 0.32

**Table 6** Partition coefficient ( $K$ ), diffusion coefficient ( $D$ ), and permeability coefficient ( $P$ ) through LSE-high after application of LC-A

	30 mM calcein	calcein-entrapped LC-A	physical mixture
LSE-high			
$K (\times 10^{-6})$	4.38	33.8	2.73
$D (\times 10^{-8} \text{ cm}^2/\text{s})$	4.52	6.20	4.71
$P (\times 10^{-1} \text{ cm/s})$	1.32	14.0	0.85

**Fig. 7** Histological observation of LSE-high 8 h after application of calcein-entrapped LC-A dispersion.

Photographs A and B are for free calcein, C and D for calcein-entrapped LC-A dispersion, and E and F for a physical mixture of free calcein and LC-A. Photographs A, C, and E show light microphotograph images, and B, D, and F show the corresponding fluorescent images. Bars indicate 100  $\mu\text{m}$  (vertical slice).

**Fig. 8** Skin viability in hairless rat intact skin and stripped skin determined by MTT assay.

Each column shows the mean  $\pm$  S.E. ( $n = 3-6$ ,  $*p < 0.05$ ).

### 3.4 Morphological observation of skin after topical application of LC-A dispersion containing calcein

Figures 7A-F show cross-sections of LSE-high 8 h after application of free calcein, calcein-entrapped LC-A, and si-

multaneous application of calcein and non-entrapped LC-A, respectively. Figures 7A, C and E show light microphotographs, and Figs. 7B, D and F show the corresponding fluorescent photographs. Similar fluorescent levels were observed for free calcein (Fig. 7B) and free calcein plus non-entrapped LC-A dispersion (Fig. 7F). In contrast, a much higher fluorescent level was found for the calcein-entrapped LC-A dispersion (Fig. 7D). These results were reflected by the skin-permeation data for LC-A dispersions (Figs. 4 and 6). Liposomes and micelles have also been found to increase the skin permeation of compounds<sup>30</sup>. It is necessary to compare the skin-permeation-enhancing effects of the present LCs with those of liposomes and micelles. This is, however, very difficult at this stage. This is because the lipids used to make LCs, liposomes, and micelles are generally different. Further trials are necessary to compare the enhancing effects of LCs, liposomes, and micelles which have all been prepared using the same or similar lipids.

### 3.5 Skin irritation by liquid-crystal formulations

Skin irritation by the LC formulations was evaluated by MTT assays in hairless rats. The obtained data for the viability of cutaneous cells are summarized in Fig. 8. No irritation (no decrease in viability) was observed for any group evaluated in this experiment when the sample was applied to intact hairless rat skin (Fig. 8a). Tape-stripped skin was used to evaluate the safety of the LC formulations. A positive control, 10% SDS, decreased the viability of skin tissue compared to the saline group. On the other hand, no decrease in viability was observed for the two LC groups (LC-A and LC-B). These results suggest that these LC formulations are safe formulation materials for skin applications.

## 4 CONCLUSION

It was found from cryo-TEM observations, electron diffraction patterns, and small-angle X-ray diffraction analysis that these LC-A and LC-B nanodispersions have reverse-hexagonal LC and cubic LC dispersions, respectively. These LC dispersions were very stable, since no aggrega-

tion (diameter growth), and little change in the LC structure (change in X-ray diffraction pattern), were observed. The entrapping ratio of a hydrophilic model compound, calcein, in LC-B was higher than that in LC-A, suggesting that cubic LC has a greater entrapping potency for hydrophilic materials. Other drugs with different lipophilicities and molecular weights must be examined in the future. The present skin-permeation experiments showed that LC-A and LC-B nanodispersions increased the skin permeation of the entrapped drug, probably as a result of increased partitioning of the LC in the skin barrier. Since the lamellar structure and lipophilicity of LCs are similar to those in the stratum corneum, the LC formulation probably increased partition of calcein into the stratum corneum, resulting in enhanced skin permeation. In addition, no skin irritation was caused by the LC dispersions.

Thus, these LC formulations can be used as new topical formulations for therapeutic drugs and cosmetic ingredients, especially for hydrophilic compounds. The content of the entrapped drugs in the skin must be determined, and detailed mechanistic analyses performed, in the near future.

#### ACKNOWLEDGEMENT

The authors thank Mr. Atsushi Kitayama and Mr. Shozo Sugitani, Terrabase Co., Ltd. for their technical assistance with Cryo-TEM observation.

#### References

- 1) Purdon, C. H.; Azzi, C. G.; Zhang, J.; Smith, E. W.; Maibach, H. I. Penetration enhancement of transdermal delivery-current permutations and limitations. *Crit. Rev. Ther. Drug Carrier Syst.* **21**, 97-132 (2004).
- 2) Kasha, P. C.; Banga, A. K. A review of patent literature for iontophoretic delivery and devices. *Recent Pat. Drug Deliv. Formul.* **2**, 41-50 (2008).
- 3) Ogura, M.; Paliwal, S.; Mitragotri, S. Low-frequency sonophoresis: Current status and future prospects. *Adv. Drug Deliv. Rev.* **60**, 1218-1223 (2008).
- 4) Tokumoto, S.; Mori, K.; Higo, N.; Sugibayashi, K. Effect of electroporation on the electroosmosis across hairless mouse skin *in vitro*. *J. Control. Release* **105**, 296-304 (2005).
- 5) Tokudome, Y.; Sugibayashi, K. Mechanism of the synergic effects of calcium chloride and electroporation on the *in vitro* enhanced skin permeation of drugs. *J. Control. Release* **95**, 267-274 (2004).
- 6) Abraham, W.; Downing, D. T. Preparation of model membranes for skin permeability studies using stratum corneum lipids. *J. Invest. Dermatol.* **93**, 809-813 (1989).
- 7) Kirjavainen, M.; Urtti, A.; Valjakka-Koskelab, R.; Kiesvaara, J.; Mönkkönen, J. Liposome-skin interactions and their effects on the skin permeation of drugs. *Eur. J. Pharm. Sci.* **7**, 279-286 (1999).
- 8) Fang, J.; Hong, C.; Chiu, W.; Wang, Y. Effect of liposomes and niosomes on skin permeation of enoxacin. *Int. J. Pharm.* **219**, 61-72 (2001).
- 9) Müller, R. H.; Mäder, K.; Gohla, S. Solid lipid nanoparticles (SLN) for controlled delivery-A review of the state of the art. *Eur. J. Pharm. Biopharm.* **50**, 161-177 (2000).
- 10) Dingler, A.; Gohla, S. Production of solid lipid nanoparticles (SLN): Scaling up feasibilities. *J. Microencapsul.* **19**, 11-18 (2002).
- 11) Geraghty, P. B.; Attwood, D.; Collett, J. H.; Sharma, H.; Dandiker, Y. An investigation of the parameters influencing the bioadhesive properties of Myverol 18-99/water gels. *Biomaterials* **18**, 63-67 (1997).
- 12) Norlén, L. Skin barrier formation, the membrane folding model. *J. Invest. Dermatol.* **117**, 823-829 (2001).
- 13) Gustafsson, J.; L-Wahren, H.; Almgren, M.; Larsson, K. Cubic lipid-water phase dispersed into submicron particles. *Langmuir* **12**, 4611-4613 (1996).
- 14) Gopal, G.; Shailendra, S.; Swarnlata, S. Cubosomes, an overview. *Biol. Pharm. Bull.* **30**, 350-353 (2007).
- 15) Barauskas, J.; Landh, T. Phase behavior of phytantriol/water system. *Langmuir* **19**, 9562-9565 (2003).
- 16) Esposito, E.; Cortesi, R.; Drechsler, M.; Paccamiccio, L.; Mariani, P.; Contado, C.; Stellin, E.; Menegatti, E.; Bonina, F.; Puglia, C. Cubosome dispersions as delivery systems for percutaneous administration of indometacin. *Pharm. Res.* **22**, 2163-2173 (2005).
- 17) Lopes, L. B.; Ferreira, D. A.; de Paula, D.; Garcia, M. T. J.; Thomazini, J. A.; Fantini, M. C. A.; Bentley, M. V. L. B. Reverse hexagonal phase nanodispersion of monoolein and oleic acid for topical delivery of peptides: *in vitro* and *in vivo* skin penetration of cyclosporin A. *Pharm. Res.* **23**, 1332-1342 (2006).
- 18) Lopes, L. B.; Lopes, J. L. C.; Oliveira, D. C. R.; Thomazini, J. A.; Garcia, M. T. J.; Fantini, M. C. A.; Collett, J. H.; Bentley, M. V. L. B. Liquid crystalline phases of monoolein and water for topical delivery of cyclosporin A, characterization and study of *in vitro* and *in vivo* delivery. *Eur. J. Pharm. Biopharm.* **63**, 146-155 (2006).
- 19) Lopes, L. B.; Speretta, F. F. F.; Bentley, M. V. L. B. Enhancement of skin penetration of vitamin K using monoolein-based liquid crystalline systems. *Eur. J. Pharm. Sci.* **32**, 209-215 (2007).
- 20) Namdeo, A.; Jain, N. K. Liquid crystalline pharmacogel based enhanced transdermal delivery of propranolol hydrochloride. *J. Control Release* **82**, 223-236 (2002).
- 21) Brinon, L.; Geiger, S.; Alard, V.; Doucet, J.; Tranchant, J. F.; Couarraze, G. Percutaneous absorption of sun-

- screens from liquid crystalline phases. *J. Control Release* **60**, 67-76 (1999).
- 22) Esposito, E.; Drechsler, M.; Mariani, P.; Sivieri, E.; Bozzini, R.; Montesi, L.; Menegatti, E.; Cortesi, R. Nanosystem for skin hydration: a comparative study. *Int. J. Cosmet. Sci.* **29**, 39-47 (2007).
- 23) Yamaguchi, Y.; Nakamura, N.; Nagasawa, T.; Kitagawa, A.; Matsumoto, K.; Soma, Y.; Matsuda, T.; Mizoguchi, M.; Igarashi, R. Enhanced skin regeneration by nanoegg formulation of all-trans retinoic acid. *Pharmazie* **61**, 117-121 (2006).
- 24) Watanabe, T.; Hasegawa, T.; Takahashi, H.; Ishibashi, T.; Takayama, K.; Sugibayashi, K. Utility of three-dimensional cultured human skin model as a tool to evaluate skin permeation of drugs. *Altern. Animal Test Experiment* **8**, 1-14 (2001).
- 25) Shah, J. C. Analysis of permeation data: evaluation of the lag time method. *Int. J. Pharm.* **90**, 161-169 (1993).
- 26) Sato, K.; Sugibayashi, K.; Morimoto, Y. Species differences in percutaneous absorption of nicorandil. *J. Pharm. Sci.* **80**, 104-107 (1991).
- 27) Watanabe, T.; Hasegawa, T.; Takahashi, H.; Ishibashi, T.; Itagaki, H.; Sugibayashi, K. Utility of MTT assay in three-dimensional cultured human skin model as an alternative for draize skin irritation test: Approach using diffusion law of irritant in skin and toxicokinetics-toxicodynamics correlation. *Pharm. Res.* **19**, 669-675 (2002).
- 28) Sugibayashi, K.; Watanabe, T.; Hasegawa, T.; Takahashi, H.; Ishibashi, T. Kinetic analysis on the *in vitro* cytotoxicity using Living Skin Equivalent for ranking the toxic potential of dermal irritants. *Toxicol. In Vitro* **16**, 759-763 (2002).
- 29) Winey, K. I.; Thomas, E. L.; Fetters, L. J. Ordered morphologies in binary blends of diblock copolymer and homopolymer and characterization of their intermaterial dividing surfaces. *J. Chem. Phys.* **95**, 9367-9375 (1991).
- 30) Rizwan, M.; Aqil, M.; Talegaonkar, S.; Azeem, A.; Sultana, Y.; Ali, A. Enhanced transdermal drug delivery techniques: An extensive review of patents. *Recent Pat. Drug Deliv. Formul.* **3**, 105-124 (2009).
-